ACS APPLIED MATERIALS & INTERFACES

Research Article

www.acsami.org

Self-Assembly Solid-State Enhanced Red Emission of Quinolinemalononitrile: Optical Waveguides and Stimuli Response

Chuanxing Shi,[†,§] Zhiqian Guo,[†,§] Yongli Yan,[‡] Shiqin Zhu,[†] Yongshu Xie,[†] Yong Sheng Zhao,*[,‡] Weihong Zhu,*[,†] and He Tian[†]

[†]Shanghai Key Laboratory of Functional Materials Chemistry, Key Laboratory for Advanced Materials and Institute of Fine Chemicals, East China University of Science and Technology, Shanghai 200237, People's Republic of China

[‡]Beijing National Laboratory for Molecular Sciences (BNLMS), Key Laboratory of Photochemistry and Institute of Chemistry, Chinese Academy of Sciences, Beijing 100190, People's Republic of China

Supporting Information

ABSTRACT: The fluorescence of luminescent emitters is often quenched in the solid state, because of the typical aggregation-caused quenching (ACQ) effect, which is a thorny obstacle to high-performance organic optoelectronic materials. The exploration of solid-state enhanced long wavelength, red-emitting chromophores, especially possessing one-dimensional (1D) assembly features, is of great importance. Interestingly, an excellent solid-state enhanced red emission system (denoted as ED) based on quinolinemalononitrile has been developed via the delicate modification of the conventional ACQ dicyanomethylene-4*H*-pyran (DCM) derivative (denoted as BD) through crystal engineering. ED exhibits extraordinary self-assembly property in a variety of solvents, even realizing the "waving ribbons" with a length of 6 mm and a diameter of 10 μm. Crystal analysis shows that the CH···π and CH···N supramolecular interactions of ED contribute to the twisted self-assembly solid-state enhanced emission phenomenon. However, for BD, strong face-to-face stacking leads to fluorescence quenching in the solid state. Because of such easy assembly and strong solid-state emission properties, application for optical waveguides of ED is realized with a low optical loss. Stimuli-responsive behavior is also elaborated with color change between orange and red by grinding/fuming or pressing/heating.

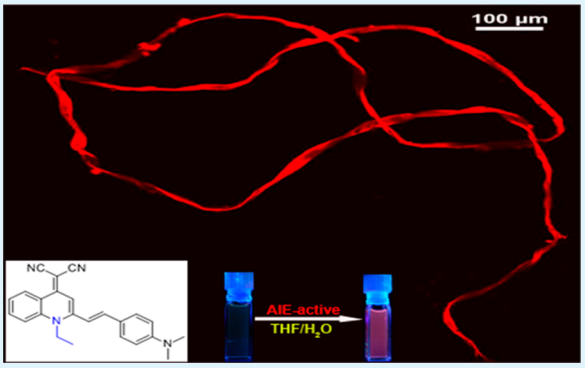

KEYWORDS: *solid-state fluorescence, self-assembly, crystal structures, optical waveguides, stimuli-response, cell imaging*

INTRODUCTION

As well-known red-emitting materials, dicyanomethylene-4*H*-pyran (DCM) derivatives have been paid much attention as highly fluorescent dopants in organic light-emitting diodes (OLEDs).[1−5] However, with the typical donor-π-acceptor (D-π-A) configuration, the conventional DCM derivatives, such as the Kodak-patented DCJTB,[2] can only be utilized as a dopant emitter, because they suffer from severe aggregation-caused quenching (ACQ) effect, which has become a thorny obstacle to the development of high-performance organic optoelectronic materials.[6] It is highly desirable to develop nondopant emitters with solid-state enhanced emission to avoid the complicated and troublesome doping process during the fabrication in OLEDs.[3,4] Recently, Tang and Park et al. observed the intriguing solid-state enhanced emission phenomenon, that is, aggregation-induced emission (AIE) or aggregation-induced enhanced emission (AIEE).[7−11] Until now, much effort has been expended toward the discovery of solid-state enhanced emission systems, mostly focused on silole, tetraphenylethene, and cyanostilbene derivatives.[7−19] As demonstrated, the strategy that tunes the intermolecular interactions associated with molecular stacking, ordering, or restriction of intramolecular rotation (RIR) in the condensed state based on rational molecular design is an efficient approach to optimize solid-state emission in organic materials.[12−15,20−30] However, solid-state enhanced long-wavelength, red-emitting systems are still rarely reported.[13,31−35] The exploration of novel solid-state enhanced red-emission chromophores, especially possessing one-dimensional (1D) assembly features, is of great importance.[36−40]

With these in mind, herein we reported a novel solid-state enhanced red emission system based on quinolinemalononitrile (denoted as ED; see Scheme 1), with an impressive alternative approach to modify the typical π-electron acceptor in DCM derivatives. Specifically, in distinct contrast with the reference compound BD[5] (see Scheme 1) with severe ACQ characteristic, quinolinemalononitrile-based ED brings several advantages, as follows: (i) showing interesting strong solid-state

Received: October 26, 2012
Accepted: December 6, 2012
Published: December 6, 2012

Scheme 1. Chemical Information Regarding ED and Reference Compound BD: (a) Chemical Structures and (b) Corresponding X-ray Single-Crystal Structures

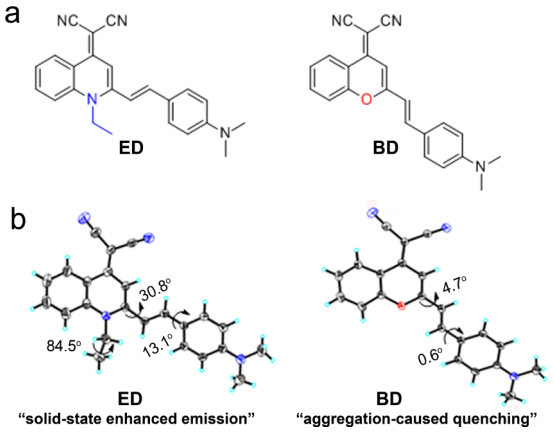

enhanced red-emission upon only replacing the oxygen atom in a 4-dicyano-methylenechromene moiety with *N*-ethyl group, (ii) easily realizing 1D micro/nanowires with the simple reprecipitation or solution evaporation methods, (iii) being suitable for organic optical waveguides with low optical loss, and (iv) exhibiting a reversibly stimuli-responsive behavior with color change between orange and red by grinding/fuming or pressing/heating. Moreover, the X-ray crystal structures of ED and BD provide a deeper insight into the solid-state enhanced emission mechanism and self-assembling behavior. Consequently, the self-assembly solid-state enhanced emission system based on quinolinemalononitrile can pave a novel pathway to design long-wavelength fluorophores for nondopant OLED emitters, bioimaging,[41−48] as well as solid-state optical waveguides.[49−53]

RESULTS AND DISCUSSION

Aggregation Behaviors of ED and BD. Tetrahydrofuran (THF) is a good solvent for both ED and BD, while water is a poor solvent. Increasing the water fraction in the THF/H_2O solution can lead to the aggregation of both dyes, that is, from isolated single molecule in THF to suspended aggregate particles (agglomerates). As shown in Figures S1 and S2 in the Supporting Information, the absorption spectra of ED were slightly affected, even if the water fraction (f_w) increases up to 70%. However, when the water fraction was further increased to 80%, the absorption intensity dropped dramatically with a long tail, indicative of forming agglomerates. Notably, the emission intensity of ED was enhanced continually with a red shift from 594 nm to 614 nm until the water fraction reached values up to 70% (see Figures 1a and 1b). The observed continuous emission enhancement and red-shift might arise from the concerted effect of an increase in the polarity of water and the resultant self-assembled agglomerates, which is similar with a polymer character.[34,54,55] The fluorescence quantum yield (Φ_F, see Table 1) exhibited an enhancement factor (defined as $\alpha_{AIE} = \Phi_{MIX}/\Phi_{THF}$) 41-fold greater than that from pure THF solution (0.1%) to the mixed THF/water (f_w = 70%) solution (4.1%). Successively, the decline with a large blue shift in the emission spectra of ED (Figure 1a) was found when the water fraction reached values up to 80%, because of the possible formation of amorphous agglomerates with random stacking structure.[14] The time effect on the aggregation showed that the absorption and emission spectra of ED (10^{-5} M) in H_2O/THF mixtures (0−70%, v/v) was almost the same when performed immediately and after 12 h (see Figure 1a and Figures S1−S3 in the Supporting Information). Interestingly, SEM images of ED prepared by THF/water mixtures (f_w = 70%) showed the typical 1D microrods ~10 μm in length

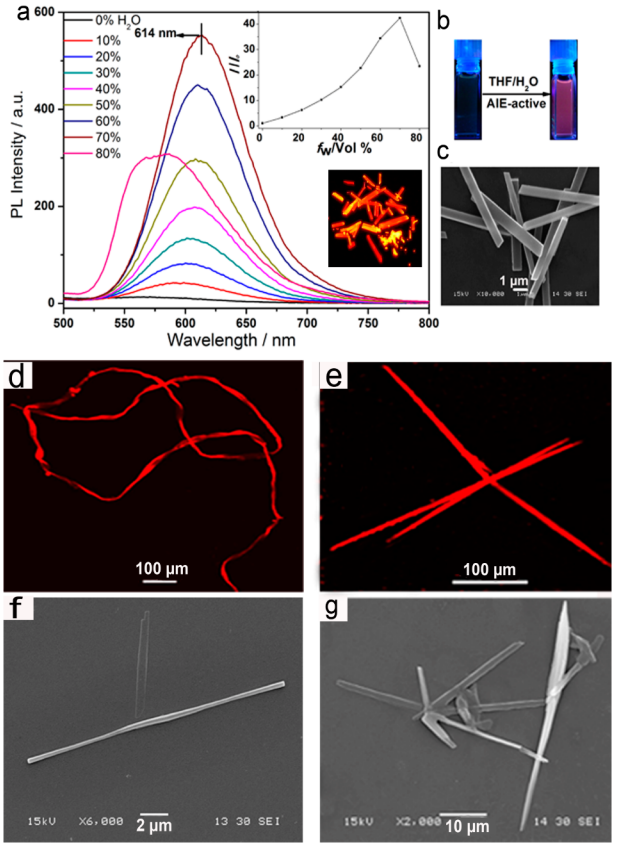

Figure 1. (a) Photoluminescence (PL) spectra of ED (10^{-5} M) in H_2O/THF mixtures with different volume fractions of water (note that the fluorescence of the resultant solution was determined after 12 h; λ_{ex} = 430 nm). Insets show a plot of relative PL intensity against water content (f_w) and a fluorescence image of microcrystal ED. (b) Fluorescence images of ED (0 and 70% H_2O) under 365-nm illumination. (c) SEM image of microrods obtained from ED suspension (70% H_2O). (d, e) Confocal fluorescence images of microwires of ED (10^{-4} M) prepared by solution evaporation method from THF solution (panel d) and from THF/EtOH (v/v = 1/1) solution (panel e). Panels f and g show their corresponding SEM images.

Table 1. Optical Properties of ED and BD[a]

	λ_{abs} [nm]	λ_{em} [nm]			
Emitter	Soln	Soln (Φ_F)[b]	Aggr (Φ_F)[b]	Film (Φ_F)[c]	Powder (Φ_F)[c]
ED	430	594 (0.1)	614 (4.1)	604 (14.7)	605 (5.2)
BD	507	636 (6.0)	693 (0.2)		

[a]Abbreviations: Soln = solution (10 μM in THF); Aggr = THF/water mixtures with 70% and 80% water fraction for ED and BD, respectively; Film = prepared through drop casting of dichloromethane solution; λ_{abs} = absorption maximum; λ_{em} = emission maximum; and Φ_F = fluorescence quantum yield. [b]Estimated using Rhodamine B as the standard (Φ_F = 50% in ethanol). Note: the optical density of the solution is <0.05, to avoid self-absorption. [c]Measured by an integrating sphere. The quantum yield of BD powder and film was too low to detect.

dx.doi.org/10.1021/am302466m | ACS Appl. Mater. Interfaces 2013, 5, 192−198

(Figure 1c), but less-ordered agglomerates were observed when the water fraction exceeded 80% (see Figure S4 in the Supporting Information). To gain further insight into the self-assembly tendency of ED, the solution evaporation method with different solvents was also employed. Red-emitting wires with different size and shape were observed under confocal fluorescence microscopy (see Figures 1d and 1e), even realizing "waving ribbons" with a length of 6 mm and a diameter of 10 μm. SEM images also indicated the forming of the nano/microrods of ED (Figure 1f and 1g). The fluorescence quantum yield of solid powder and film for ED was determined with 5.2% and 14.7%, respectively (Table 1). Obviously, ED has both typical solid-state enhanced emission and 1D self-assembly features.

In contrast, DCM-based BD demonstrates a totally opposite phenomenon with ACQ effect (Figure S5 in the Supporting Information). With the increasing water fraction in mixed solution from 0% to 70%, the absorption peak red-shifted by 33 nm from 507 nm to 540 nm. When the water fraction was up to 80%, the absorption peak was abruptly blue-shifted by ~52 nm, with the absorption tail extending into the long-wavelength region (see Figure S6 in the Supporting Information). Although the fluorescence intensity of BD increased initially from pure THF solution to f_w = 10%, it became quenched to almost zero continuously. In fact, the fluorescence quantum yield has a 30-fold decrease from 6.0% to 0.2%, with respect to the isolated single molecule state in THF (see Table 1 and Figure S7 in the Supporting Information). Also, SEM images further confirmed the predominated existence of lamellar agglomerates (Figure 2b, inset) at f_w = 80%.

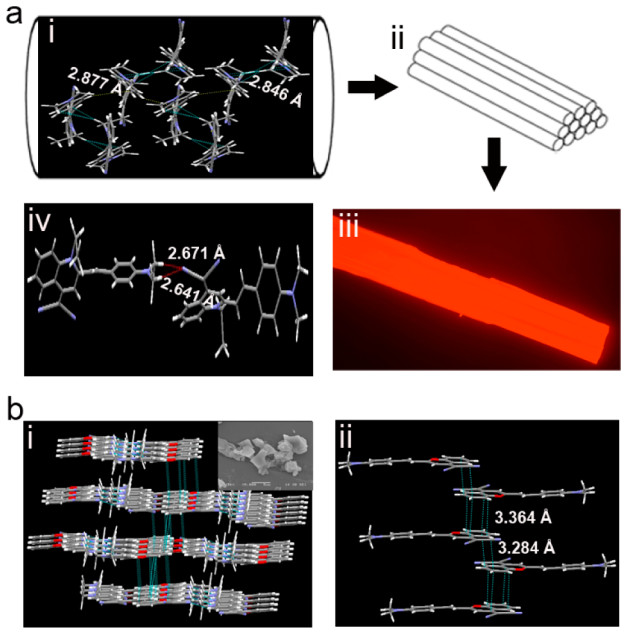

Figure 2. (a) Images describing the chemistry of ED: (i) Cross-stacking molecules in one-dimensional (1D) molecular column through CH···π weak interactions, (ii) proposed stacking of 1D molecular column, (iii) the crystal image under fluorescence microscopy, and (iv) the interaction between columns through CH···N weak interactions in single-crystal X-ray analysis. (b) Images describing the chemistry of BD: (i) Molecular stacking diagram (inset shows the formation of lamellar agglomerates at 80% water fraction) and (ii) the intermolecular π···π interactions.

From the viewpoint of chemical structures, both ED and BD are D-π-A systems, but the intramolecular charge transfer (ICT) extent from donor to acceptor is different.[56,57] Actually, ED and BD show the solvent effect to different extents (see Table S1 and Figure S8 in the Supporting Information). Upon increasing the solvent polarity, the absorption band of BD exhibits a red shift by 38 nm (from 475 nm in hexane to 513 nm in ethanol), accompanied by a red shift by 76 nm in the emission spectra (from 584 nm in toluene to 660 nm in ethanol). In contrast, ED shows less solvent effect with slight absorption peak changes, thus indicating that the introduction of *N*-ethyl group in the acceptor of ED might decrease the ICT process with a smaller solvent effect. Also, from the density functional theory (DFT) results, the structure of BD takes an almost-planar conformation, while ED takes a twisted conformation in isolated state (see Figure S9 in the Supporting Information). In addition, BD shows a more obvious shift in electron density than ED does when the molecules are excited from the highest occupied molecular orbital (HOMO) to the lowest unoccupied orbital (LUMO). Moreover, the HOMO orbital levels for ED and BD are almost the same, the predominant difference is on the LUMO orbital; that is, the LUMO of ED is 0.44 eV higher than that of BD, which is indicative of the weaker electron-withdrawing ability of quinolinemalononitrile or a torsional structure of ED (see Table S2 in the Supporting Information). It is suggested that the active intramolecular rotation and torsional induced intermolecular collision can deactivate the excited state through nonradiative relaxation.[9,58,59] Accordingly, in ED, the torsional induced intermolecular interactions and the rotation of aromatic ring (rotor: quinoline and phenyl ring) through the C−C single bond linked to the ethylene core (stator) will lead to higher nonradiative deactivation than that of BD in pure THF solution. However, the deactivation process in BD might be restricted by the strong push−pull strength and planar conformation. Therefore, ED emits faintly, while BD emits intensely in pure THF solution.

Crystal Analysis. Now, the question is why quinolinemalononitrile-based ED shows the interesting characteristic of self-assembly solid-state enhanced emission upon aggregation when replacing the oxygen atom in 4-dicyano-methylenechromene moiety with *N*-ethyl group, which is in contrast with the severe ACQ effect of DCM-based BD. Fortunately, both single crystals of ED and BD were obtained through the slow evaporation of dichloromethane/hexane (v/v = 1:1) mixtures (see Table S3 in the Supporting Information), showing different molecular stacking arrangements, which could give rise to different solid-state emission properties.[12] As shown in Scheme 1, the single-crystal X-ray structure confirms the *trans* conformation in both ED and BD. Moreover, quinolinemalononitrile unit takes a larger angle with the central ethylene unit, because of the repulse of the *N*-ethyl group with the central ethylene unit. The double-bond length of the central ethylene unit connecting donor and acceptor units is almost the same (1.33 Å) for both ED and BD, indicating that the sp^2-sp^2 hybridization of the C=C double bond is not affected so much with the bridging donor and acceptor. ED takes a twisted conformation with a torsional angle of 30.8° (between the central ethylene and quinoline units) and 13.1° (between the central ethylene and phenyl ring), respectively. Furthermore, the *N*-ethyl group has a torsional angle of 84.5° from the quinoline plane. In such a twisted structure, there exists a specific intermolecular CH···π interaction between the methylene hydrogen ($-NCH_2-$) and

dx.doi.org/10.1021/am302466m | ACS Appl. Mater. Interfaces 2013, 5, 192−198

phenyl group cooperatively with interaction between phenyl-H and ethylene unit (Figure 2a), thus inducing ED molecules to self-assemble into 1D columns with a T-type short contact between neighboring stacking molecules (H···π distances of 2.846 Å and 2.877 Å), which can greatly decrease the face-to-face π···π stacking. Also, there exists weak CH···N head-to-tail *J*-type interaction (H···N distances of 2.671 Å and 2.641 Å) between columns (Figure 2a(iv)). Such supramolecular bonding interactions can suppress the rotation or motion of ED molecules and induce the molecules to form 1D ordered micro/nanostructures, thus leading to macroscopic self-assembly solid-state enhanced emission, which is a key element for optical waveguides.[52]

In contrast, as shown in Figure 2b, BD takes a planar structure, with small torsional angles of 0.6° and 4.7° under the CH···N and dipole−dipole interactions. The strong π···π interaction between aromatic ring (closest C···C distances of 3.284 and 3.364 Å) leads to strong face-to-face stacking with a typical ACQ effect in the solid state. Taken together, the easily self-assembled 1D micro/nanowires of ED with strong solid-state enhanced emission are essentially due to the incorporation of *N*-ethyl group into 4-dicyano-methylenechromene moiety, resulting in a twisted conformation with head-to-tail *J*-type aggregation during the self-assembly process. Upon aggregation, the nonradiative deactivation through the torsional conformation and the close π···π stacking of ED molecules can be efficiently suppressed. As a consequence, the controlled crystal engineering through different molecular stacking of ED and BD might play a great role in the different macroscopic solid-state emission behaviors.

Optical Waveguides. Because of the easy self-assembly and solid-state enhanced emission property of ED, we explored its application for organic optical waveguiding.[49−53] We used photoluminescence (PL) microscopy (Figure 3a) to study the optical waveguide properties of ED nanorods. When we excited the middle of the nanorod with a focused laser beam, the resulting PL of ED was strong enough to be guided to the ends of the nanorod (Figure 3a). To measure the microarea PL spectra of single nanorods, we excited the nanorods dispersed on a glass coverslip with a UV laser (351 nm, Beamlok, Spectra-physics). The excitation laser was filtered with a band-pass filter (330−380 nm), then focused to excite the nanorods with an objective (CF LU Plan Epi 50X, Nikon). The spot size was <2 μm. The collected PL emission was coupled to a grating spectrometer (Acton, Model SP-2358) with a matched ProEm: 1600×200 B EMCCD camera (Princeton Instruments). Figure 3b displays the spatially resolved spectra of the waveguided emission that is outcoupled at a nanorod tip, and Figure 3c exhibits the output intensity as a function of propagation length, respectively. The optical loss coefficient (α) was calculated by a single exponential fitting ($I_{tip}/I_{body} = A \exp^{-\alpha x}$, where x is the distance between the exciting site and the emitting tip and A is the ratio of the light escaping from the excitation spot, relative to the light propagating along the rod). The I_{body} term was adopted as a reference to reduce the time fluctuation of the input laser. Here, α was determined to be 0.287 dB/μm. No obvious spectrum shift was observed with the increase in propagation distances (Figure 3b). Hence, the overlap of the absorption and fluorescence spectra is negligible, which is a main factor for such a low-loss optical waveguide. Despite the reduced reabsorption, the smooth surface and distinctly flat end facets also minimized the optical loss caused by scattering, contributing to the excellent optical waveguide behaviors.

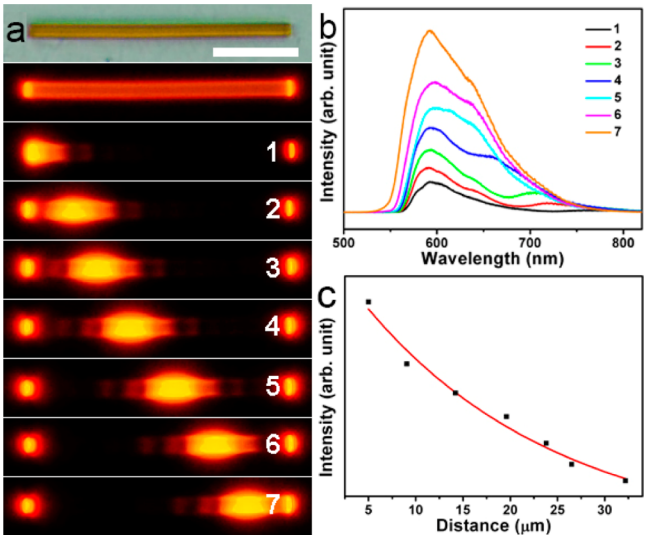

Figure 3. (a) Microscope images and the corresponding PL microscopy images of ED crystal, (b) the spatial resolved spectra of the waveguided emission that is outcoupled by excitation at distances of 32.2, 26.5, 23.8, 19.6, 14.2, 9.05, and 5 μm from the tip of a single nanorod (numbered 1−7 in panel a), and (c) the output intensity as a function of propagation length, respectively. [Note: Scale bar = 10 μm. The red area was excited by focused laser light (λ_{ex} = 351 nm).]

Stimuli Response. Actually, the morphology or stacking arrangement of the aggregate can be easily tuned by external stimuli such as pressure, heat, and vapor. These unique features would provide potential applications for smart materials as sensors and memory chips.[10,60−65] The stimuli-responsive behavior of ED was realized by grinding/fuming or pressing/heating. The pristine powder of ED (T_d = 328 °C) emitted a strong orange light with a peak centered at 605 nm (upon excitation with 365-nm UV light). After being pressed or ground, a bright red emission with a red shift of ~40 nm occurred, with a fluorescence peak at 645 nm, arising from more tightly stacking with the increased $\pi-\pi$ interaction.[65] Moreover, the ground sample could be almost recovered to the original state by annealing or fuming (see Figure 4a and Figures S10−S11 in the Supporting Information). Both differential scanning calorimetry (DSC) and X-ray diffraction (XRD) curves verified the different aggregate morphology of ED. According to DSC measurements, the thermogram of ground powder exhibited a crystallization temperature at 101 °C, which was not observed for the pristine or annealed sample (Figure 4b), indicating that the ground sample exists in a metastable amorphous state. For XRD, the diffraction curves of pristine powder possessed sharp and intense reflections, while disappeared or weakened through grinding or pressing (Figure 5), indicating the transformation of crystalline state to amorphous state to some extent.[62]

Cell Imaging. Since the π-conjugated dyes loaded on the cellular membrane easily result in concentration quenching, highly fluorescent nanoparticles have been used for bioimaging to avoid this problem.[28,41−48] The nonradiative emission will be suppressed in a cellular environment, because of the restricted motion of the molecule ascribed from the high viscosity in cell or hydrophobic effect. Herein, ED with a strong solid-state red emission in an aggregated state also successfully served as a bioimaging agent in aqueous media with bright red emission at

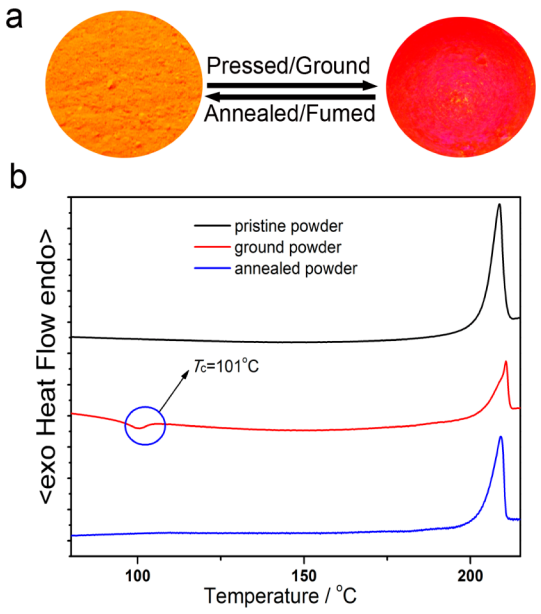

Figure 4. (a) Photographic images of ED powder under 365-nm UV light: pristine, ground (grinding pristine powder with pestle), annealed (ground powder annealed at 100 °C for 5 min), and fumed (reground powder in dichloromethane vapor for 5 min). (b) DSC curves of pristine, ground, annealed powder of ED under nitrogen. (Scan rate = 20 °C min^{-1}.)

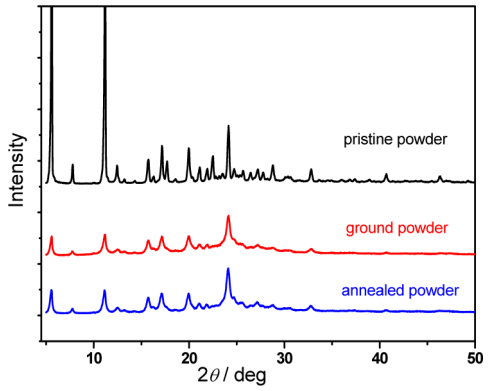

Figure 5. Powder X-ray diffraction (XRD) patterns of pristine, ground, and annealed powder of ED.

cellular cytoplasms, which can avoid the strong interference from the UV-induced phototoxicity/autofluorescence. As shown in the cell imaging (Figure 6), ED nanoaggregates can easily penetrate the cell membranes, probably through an endocytosis process. While almost no fluorescence is observed in the cell nucleus, possibly because of the large size of the nanoparticle. Meanwhile, bright-field image measurement confirmed that the cell were viable throughout the imaging studies.

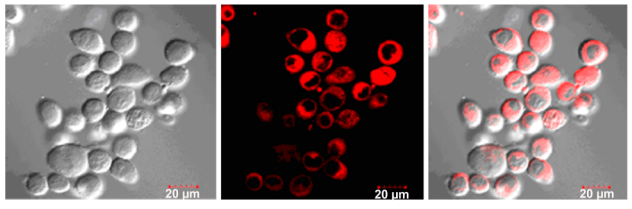

Figure 6. Confocal fluorescence images in KB cells incubated with a PBS solution of ED (10^{-5} M) for 0.5 h. From left to right: bright-field image, fluorescence image, and overlap field image. Emission was collected at 565−665 nm.

CONCLUSIONS

In summary, a novel solid-state enhanced red-emission emitter ED with self-assembly properties has been presented through controlled crystal engineering, by the subtle modification of the six-membered heterocycle DCM derivative with *N*-ethyl group. The introduction of *N*-ethyl group on the acceptor of quinolinemalononitrile can result in a twisted conformation with head-to-tail *J*-type aggregation during the self-assembly process, thus efficiently suppressing the nonradiative deactivation through the torsional conformation and the close stacking of molecules in the solid state. Moreover, on the basis of the CH···π and CH···N supramolecular interactions, ED adds the solid-state enhanced emission family with several benefits, such as the long wavelength, strong red-emission, self-assemble into 1D micro/nanowires, highly efficient optical waveguides, and a reversibly stimuli-responsive behavior with color change between orange and red by grinding/fuming or pressing/heating. Novel solid-state enhanced emission based on ED derivatives with long emission and recognizing subunit are in progress, especially for bioimaging and electroluminescent materials.

EXPERIMENTAL SECTION

Materials and General Methods. THF was distilled under argon atmosphere from sodium benzophenone ketyl immediately prior to use. All other solvents and chemicals were purchased commercially, and used as received without further purification. The ^{1}H and ^{13}C NMR spectra were obtained with a Bruker Model AM 400 spectrometer (relative to tetramethylsilane (TMS)). High-resolution mass spectra measurements were carried out using a Waters LCT Premier XE spectrometer, and UV-vis spectra were performed on a Varian Cary 500 spectrophotometer. Fluorescence spectra were recorded on a Varian Cary Eclipse fluorescence spectrophotometer. Quantum yields of the solid samples were recorded on a Horiba Model Fluoromax 4 system with a calibrated intergrating sphere. Scanning electron microscopy (SEM) micrographs were obtained on a JEOL Model JSM-6360 SEM microscope. Confocal fluorescence images were taken on an inverted fluorescence microscope (Nikon Model A1R/A1). The differential scanning calorimetry (DSC) analysis was performed under a nitrogen atmosphere on a TA Instruments DSC 2920 system. Thermogravimetric analysis (TGA) was undertaken using a Perkin−Elmer Model Pyris 1 thermogravimetric analyzer. The X-ray diffraction (XRD) intensity data were collected at 293 K on a Rigaku RAXIS RAPID IP imaging plate system with Mo Kα radiation (λ = 0.71073 Å). For the measurement of waveguide property, a discrete wire was locally excited with a focused 351-nm Ar^{+}-ion laser (Spectra-Physics Beamlok). The spatially resolved spectra were collected with a grating spectrometer (Princeton Instruments). The commercial rotating filter block (Nikon MBE41200: EX330-380, DM400, and BA420) was used in all optical microscopy and microspectroscopic measurements to remove the excitation light.

Preparation of Nanoaggregates. Stock THF solutions of compounds ED and BD with a concentration of 10^{-4} M were prepared. Aliquots of the stock solution were transferred to 10-mL volumetric flasks. After appropriate amounts of THF were added, water was added dropwise under vigorous stirring to furnish 10^{-5} M solutions with different water contents (f_w = 0−80 vol %). The absorption and PL measurements of the resultant solutions were then performed immediately and after 12 h. Nanoaggregates of SEM images were prepared by the slow evaporation of one drop of the suspension (performed after 12 h) on quartz plate.

dx.doi.org/10.1021/am302466m | *ACS Appl. Mater. Interfaces* 2013, 5, 192−198

Synthesis. As shown in Scheme S1 in the Supporting Information, compounds ED and BD were prepared through Knoevenagel reactions.

1-Ethyl-2-(4-dimethylaminostyryl)-4-(dicyanomethylene)-1,4-dihydroquinoline (ED). 1-Ethyl-2-methyl-4-(dicyanomethylene)-1,4-dihydroquinoline (1.0 g, 4.2 mmol) and 4-dimethylaminobenzaldehyde (0.7 g, 4.6 mmol) was dissolved in 35 mL of toluene with piperidine (1.0 mL) and acetic acid (0.5 mL) under argon protection at room temperature. The mixture then was refluxed for 12 h. The solvent was removed under reduced pressure, and the crude product was purified by silica gel chromatography with dichloromethane/petroleum ether (5:1) to afford the desired product (0.7 g, 1.9 mmol) as orange solid: yield = 45%. ^{1}H NMR (400 MHz, $CDCl_3$, ppm): δ = 1.56 (t, J = 7.2 Hz, 3H, $-CH_2CH_3$), 3.04 (s, 6H, $-CH_3$), 4.38 (q, J = 7.2 Hz, 2H, $-CH_2CH_3$), 6.70 (d, J = 8.8 Hz, 2H, phenyl−H), 6.80 (d, J = 16.0 Hz, 1H, alkene−H), 7.15 (s, 1H, quinoline−H), 7.29 (d, J = 16.0 Hz, 1H, alkene−H), 7.40−7.46 (m, 3H, phenyl−H), 7.60 (d, J = 8.8 Hz, 1H, phenyl−H), 7.73 (t × d, J_1 = 8.0 Hz, J_2 =1.6 Hz, 1H, phenyl−H), 9.11 (d, J = 8.4 Hz, 1H, phenyl−H). ^{13}C NMR (100 MHz, $CDCl_3$, ppm): δ = 13.94, 40.16, 43.77, 49.72, 107.00, 111.95, 112.27, 113.25, 116.00, 119.70, 120.80, 121.60, 122.69, 124.37, 126.93, 129.37, 129.54, 132.93, 138.21, 141.02, 148.85, 151.65, 153.12. Mass spectrometry (ESI positive ion mode for $[M + H]^+$): Calcd. for $C_{24}H_{22}N_4$: 367.1923; Found: 367.1929.

4-(Dicyanomethylene)-2-(4-dimethylaminostyryl)chromone (BD). BD was synthesized using the same method for ED with 4-(dicyanomethylene)-2-methyl-chromone and 4-dimethylaminobenzaldehyde. A dark red solid (500 mg, 1.5 mmol) was obtained: Yield = 56%. ^{1}H NMR (400 MHz, $CDCl_3$, ppm): δ = 3.07 (s, 6H, $-CH_3$), 6.58 (d, J = 16.0 Hz, 1H, alkene−H), 6.71 (t, J = 8.8 Hz, 2H, phenyl−H), 6.78 (s, 1H, pyran−H), 7.42 (t, J = 8.0 Hz, 1H, phenyl−H), 7.48 (d, J = 8.8 Hz, 2H, phenyl−H), 7.52 (d × d, J_1 = 8.4 Hz, J_2 = 1.2 Hz, 1H, phenyl−H), 7.57 (d, J = 16.0 Hz, 1H, alkene−H), 7.70 (t × d, J_1 = 8.0 Hz, J_2 = 1.2 Hz, 1H, phenyl−H), 8.91 (d × d, J = 8.4 Hz, 1.2 Hz, 1H, phenyl−H). ^{13}C NMR (100 MHz, $CDCl_3$, ppm): δ = 158.94, 152.77, 152.41, 151.96, 139.87, 134.15, 129.94, 125.75, 125.57, 122.42, 118.42, 118.03, 117.50, 116.42, 112.88, 111.96, 105.27, 60.15, 40.11, 29.71. Mass spectrometry (ESI positive ion mode for $[M + H]^+$): Calcd. for $C_{22}H_{18}N_3O$: 340.1450; Found: 340.1447.

■ ASSOCIATED CONTENT

Ⓢ Supporting Information

Spectroscopic properties and crystallographic data for ED (CCDC 881659) and BD (CCDC 881660), obtained from Cambridge Crystallographic Data Centre (CCDC). This material is available free of charge via the Internet at http://pubs.acs.org.

■ AUTHOR INFORMATION

Corresponding Author

*Fax: (+86) 21-6425-2758 (W.Z.), (+86) 10-6265-2029 (Y.S.Z.). E-mail: whzhu@ecust.edu.cn (W.Z.), yszhao@iccas.ac.cn (Y.S.Z.).

Author Contributions

§C.X.S. and Z.Q.G. contributed equally to this work.

Notes

The authors declare no competing financial interest.

■ ACKNOWLEDGMENTS

This work was supported by NSFC/China, National 973 Program (No. 2013CB733700), the Oriental Scholarship (No. SRFDP 200802510011), the Fundamental Research Funds for the Central Universities (Nos. WK1013002, WJ1114013), STCSM (No. 10dz2220500), and the Open Funding Project of State Key Laboratory of Luminescent Materials and Devices (SCUT) for providing financial support to this project. Helpful discussion with Dr. Z. Y. Zhang and Q. Zhang was greatly appreciated.

■ REFERENCES

(1) Tang, C. W.; VanSlyke, S. A.; Chen, C. H. *J. Appl. Phys.* **1989**, *65*, 3610−3616.
(2) Chen, C. H.; Klubek, K. P.; Shi, J. M. U.S. Patent 5,908,581, June 1, 1999.
(3) Chen, C. T. *Chem. Mater.* **2004**, *16*, 4389−4400.
(4) Guo, Z. Q.; Zhu, W. H.; Tian, H. *Chem. Commun.* **2012**, *48*, 6073−6084.
(5) Ermer, S.; Lovejoy, S. M.; Leung, D. S.; Warren, H.; Moylan, C. R.; Twieg, R. J. *Chem. Mater.* **1997**, *9*, 1437−1442.
(6) Valeur, B. *Molecular Fluorescence: Principles and Applications*; Wiley−VCH Verlag GmbH, 2001; p 72.
(7) Luo, J.; Xie, Z.; Lam, J. W. Y.; Cheng, L.; Chen, H.; Qiu, C.; Kwok, H. S.; Zhan, X.; Liu, Y.; Zhu, D.; Tang, B. Z. *Chem. Commun.* **2001**, 1740−1741.
(8) An, B.-K.; Kwon, S.; Jung, S.; Park, S. Y. *J. Am. Chem. Soc.* **2002**, *124*, 14410−14415.
(9) Hong, Y.; Lam, J. W. Y.; Tang, B. Z. *Chem. Soc. Rev.* **2011**, *40*, 5361−5388.
(10) Ning, Z.; Chen, Z.; Zhang, Q.; Yan, Y.; Qian, S.; Cao, Y.; Tian, H. *Adv. Funct. Mater.* **2007**, *17*, 3799−3807.
(11) Würthner, F.; Kaiser, T. E.; Saha-Möller, C. R. *Angew. Chem. Int. Ed.* **2011**, *50*, 3376−3410.
(12) An, B.-K.; Gierschner, J.; Park, S. Y. *Acc. Chem. Res.* **2012**, *45*, 544−554.
(13) An, B.-K.; Gihm, S. H.; Chung, J. W.; Park, C. R.; Kwon, S.; Park, S. Y. *J. Am. Chem. Soc.* **2009**, *131*, 3950−3957.
(14) Yoon, S.; Park, S. Y. *J. Mater. Chem.* **2011**, *21*, 8338−8346.
(15) Kim, S.; Yoon, S.; Park, S. Y. *J. Am. Chem. Soc.* **2012**, *134*, 12091−12097.
(16) Wang, M.; Zhang, G.; Zhang, D.; Zhu, D.; Tang, B. Z. *J. Mater. Chem.* **2010**, *20*, 1858−1867.
(17) Shimizu, M.; Hiyama, T. *Chem. Asian J.* **2010**, *5*, 1516−1531.
(18) Sun, F.; Zhang, G. X.; Zhang, D.; Xue, L.; Jiang, H. *Org. Lett.* **2011**, *13*, 6378−6381.
(19) Nakamura, M.; Sanji, T.; Tanaka, M. *Chem.—Eur. J.* **2011**, *17*, 5344−5349.
(20) Varghese, S.; Das, S. *J. Phys. Chem. Lett.* **2011**, *2*, 863−873.
(21) Li, R. J.; Hu, W. P.; Liu, Y. Q.; Zhu, D. B. *Acc. Chem. Res.* **2010**, *43*, 529−540.
(22) Javed, I.; Zhou, T.; Muhammad, F.; Guo, J.; Zhang, H.; Wang, Y. *Langmuir* **2012**, *28*, 1439−1446.
(23) Upamali, K. A. N.; Estrada, L. A.; De, P. K.; Cai, X.; Krause, J. A.; Neckers, D. C. *Langmuir* **2011**, *27*, 1573−1580.
(24) Xie, Z.; Yang, B.; Li, F.; Cheng, G.; Liu, L.; Yang, G.; Xu, H.; Ye, L.; Hanif, M.; Liu, S.; Ma, D.; Ma, Y. *J. Am. Chem. Soc.* **2005**, *127*, 14152−14153.
(25) Ghodbane, A.; D'Altério, S.; Saffon, N.; McClenaghan, N. D.; Scarpantonio, L.; Jolinat, P.; Fery-Forgues, S. *Langmuir* **2012**, *28*, 855−863.
(26) Chen, H. Y.; Chi, Y.; Liu, C. S.; Yu, J. K.; Cheng, Y. M.; Chen, K. S.; Chou, P. T.; Peng, S. M.; Lee, G. H.; Carty, A. J.; Yeh, S. J.; Chen, C. T. *Adv. Funct. Mater.* **2005**, *15*, 567−574.
(27) Zhao, Z.; Chen, S.; Lam, J. W. Y.; Lu, P.; Zhong, Y.; Wong, K. S.; Kwok, H. S.; Tang, B. Z. *Chem. Commun.* **2010**, *46*, 2221−2223.
(28) Qin, W.; Ding, D.; Liu, J.; Yuan, W. Z.; Hu, Y.; Liu, B.; Tang, B. Z. *Adv. Funct. Mater.* **2012**, *22*, 771−779.
(29) Zhao, Z.; Lam, J. W. Y.; Chan, C. Y. K.; Chen, S.; Liu, J.; Lu, P.; Rodriguez, M.; Maldonado, J.; Ramos-Ortiz, G.; Sung, H. H. Y.; Williams, I. D.; Su, H.; Wong, K. S.; Ma, Y.; Kwok, H. S.; Qiu, H.; Tang, B. Z. *Adv. Mater.* **2011**, *23*, 5430−5435.
(30) Hong, Y.; Lam, J. W. Y.; Tang, B. Z. *Chem. Commun.* **2009**, 4332−4353.
(31) Shimizu, M.; Kaki, R.; Takeda, Y.; Hiyama, T.; Nagai, N.; Yamagishi, H.; Furutani, H. *Angew. Chem., Int. Ed.* **2012**, *51*, 4095−4099.

(32) Zhang, Z.; Xu, B.; Su, J.; Shen, L.; Xie, Y.; Tian, H. *Angew. Chem., Int. Ed.* **2011**, *50*, 11654−11657.
(33) Zhao, Z. J.; Geng, J. L.; Chang, Z. F.; Chen, S. M.; Deng, C. M.; Jiang, T.; Qin, W.; Lam, J. W. Y.; Kwok, H. S.; Qiu, H. Y.; Liu, B.; Tang, B. Z. *J. Mater. Chem.* **2012**, *22*, 11018−11021.
(34) Tong, H.; Hong, Y.; Dong, Y.; Ren, Y.; Häussler, M.; Lam, J. W. Y.; Wong, S. K.; Tang, B. Z. *J. Phys. Chem. B* **2007**, *111*, 2000−2007.
(35) Lee, Y.; Chiang, C.; Chen, C. *Chem. Commun.* **2008**, 217−219.
(36) Grimsdale, A. C.; Müllen, K. *Angew. Chem., Int. Ed.* **2005**, *44*, 5592−5629.
(37) Zang, L.; Che, Y.; Moore, J. S. *Acc. Chem. Res.* **2008**, *41*, 1596−1608.
(38) Zhao, Y. S.; Fu, H.; Peng, A.; Ma, Y.; Liao, Q.; Yao, J. N. *Acc. Chem. Res.* **2010**, *43*, 409−418.
(39) Jiang, L.; Dong, H. L.; Hu, W. P. *Soft Matter* **2011**, *7*, 1615−1630.
(40) Ajayaghosh, A.; Praveen, V. K. *Acc. Chem. Res.* **2007**, *40*, 644−656.
(41) Kobayashi, H.; Ogawa, M.; Alford, R.; Choyke, P. L.; Urano, Y. *Chem. Rev.* **2010**, *110*, 2620−2640.
(42) Zhao, Q.; Huang, C.; Li, F. *Chem. Soc. Rev.* **2011**, *40*, 2508−2524.
(43) Chen, X.; Nam, S.; Kim, G.; Song, N.; Jeong, Y.; Shin, I.; Kim, S. K.; Kim, J.; Park, S.; Yoon, J. *Chem. Commun.* **2010**, *46*, 8953−8955.
(44) Peng, X. J.; Yang, Z. G.; Y., J.; Fan, J. L.; He, Y. X.; Song, F. L.; Wang, B. S.; Sun, S. G.; Qu, J. L.; Qi, J.; Yang, M. *J. Am. Chem. Soc.* **2011**, *133*, 6626−6635.
(45) Guliyev, R.; Coskun, A.; Akkaya, E. U. *J. Am. Chem. Soc.* **2009**, *131*, 9007−9013.
(46) Oushiki, D.; Kojima, H.; Terai, T.; Arita, M.; Hanaoka, K.; Urano, Y.; Nagano, T. *J. Am. Chem. Soc.* **2010**, *132*, 2795−2801.
(47) Wu, W. H.; Ji, S. M.; Wu, W. T.; Shao, J. Y.; Guo, H. M.; James, T. D.; Zhao, J. Z. *Chem.—Eur. J.* **2012**, *18*, 4953−4964.
(48) Pluth, M. D.; Chan, M. R.; McQuade, L. E.; Lippard, S. J. *Inorg. Chem.* **2011**, *50*, 9385−9392.
(49) Yanagi, H.; Ohara, T.; Morikawa, T. *Adv. Mater.* **2001**, *13*, 1452−1455.
(50) O'Carroll, D.; Lieberwirth, I.; Redmond, G. *Small* **2007**, *3*, 1178−1183.
(51) Liu, T.; Li, Y.; Yan, Y.; Li, Y.; Yu, Y.; Chen, N.; Chen, S.; Liu, C.; Zhao, Y. S.; Liu, H. *J. Phys. Chem. C* **2012**, *116*, 14134−14138.
(52) Xu, Y.; Zhang, H.; Li, F.; Shen, F.; Wang, H.; Li, X.; Yu, Y.; Ma, Y. *J. Mater. Chem.* **2012**, *22*, 1592−1597.
(53) Tavazzi, S.; Borghesi, A.; Papagni, A.; Spearman, P.; Silvestri, L.; Yassar, A.; Caamposeo, A.; Polo, M.; Pisignano, D. *Phys. Rev. B* **2007**, *75*, 245416.
(54) Mei, J.; Wang, J.; Sun, J. Z.; Zhao, H.; Yuan, W.; Deng, C.; Chen, S.; Sung, H. H. Y.; Lu, P.; Qin, A.; Kwok, H. S.; Ma, Y.; Williams, I. D.; Tang, B. Z. *Chem. Sci.* **2012**, *3*, 549−558.
(55) Yuan, W. Z.; Yu, Z.; Lu, P.; Deng, C.; Lam, J. W. Y.; Wang, Z.; Chen, E.; Ma, Y.; Tang, B. Z. *J. Mater. Chem.* **2012**, *22*, 3323−3326.
(56) Lackowicz, J. R. In *Principles of Fluorescence Spectroscopy*, 3rd Edition; Springer: New York, 2006; Vol. *6*, pp 205−235.
(57) Grabowski, Z. R.; Rotkiewicz, K.; Rettig, W. *Chem. Rev.* **2003**, *103*, 3899−4032.
(58) Oelkrug, D.; Tompert, A.; Gierschner, J.; Egelhaaf, H.; Hanack, M.; Hohloch, M.; Steinhuber, E. *J. Phys. Chem. B* **1998**, *102*, 1902−1907.
(59) Kwon, J. E.; Park, S. Y. *Adv. Mater.* **2011**, *23*, 3615−3642.
(60) Sagara, Y.; Kato, T. *Nat. Chem.* **2009**, *1*, 605−610.
(61) Kunzelman, J.; Kinami, M.; Crenshaw, B. R.; Protasiewicz, J. D.; Weder, C. *Adv. Mater.* **2008**, *20*, 119−122.
(62) Chi, Z.; Zhang, X.; Xu, B.; Zhou, X.; Ma, C.; Zhang, Y.; Liu, S.; Xu, J. *Chem. Soc. Rev.* **2012**, *41*, 3878−3896.
(63) Luo, X.; Li, J.; Li, C.; Heng, L.; Dong, Y. Q.; Liu, Z.; Bo, Z.; Tang, B. Z. *Adv. Mater.* **2011**, *23*, 3261−3265.
(64) Yoon, S.; Chung, J. W.; Gierschner, J.; Kim, K. S.; Choi, M.; Kim, D.; Park, S. Y. *J. Am. Chem. Soc.* **2010**, *132*, 13675−13683.
(65) Dong, Y.; Xu, B.; Zhang, J.; Tan, X.; Wang, L.; Chen, J.; Lv, H.; Wen, S.; Li, B.; Ye, L.; Zou, B.; Tian, W. *Angew. Chem., Int. Ed.* **2012**, *51*, 10782−10785.